Losing supramolecular orientational memory *via* self-organization of a misfolded secondary structure

Journal:	*Polymer Chemistry*
Manuscript ID	PY-ART-02-2018-000187.R1
Article Type:	Paper
Date Submitted by the Author:	16-Mar-2018
Complete List of Authors:	Sahoo, Dipankar; University of Pennsylvania Peterca, Mihai; University of Pennsylvania, Department of Chemistry Aqad, Emad; University of Pennsylvania Partridge, Benjamin; University of Pennsylvania, Department of Chemistry Klein, Michael; Temple University, Chemistry Percec, Virgil; University of Pennsylvania,

Losing supramolecular orientational memory *via* self-organization of a misfolded secondary structure

Dipankar Sahoo,[a] Mihai Peterca,[a,b] Emad Aqad,[a] Benjamin E. Partridge,[a] Michael L. Klein,[c] and Virgil Percec*[a]

[a] *Roy & Diana Vagelos Laboratories, Department of Chemistry, University of Pennsylvania, Philadelphia, Pennsylvania 19104-6323, United States*

[b] *Department of Physics and Astronomy, University of Pennsylvania, Philadelphia, Pennsylvania 19104-6396, United States*

[c] *Institute of Computational Molecular Science, Temple University, Philadelphia, Pennsylvania 19122, United States*

**E-mail: percec@sas.upenn.edu*

Supramolecular orientational memory (SOM) provides a route to otherwise inaccessible nanoscale architectures for certain molecules. In these privileged cases, columnar domains organized from self-assembling dendrons undergo reorientation during heating to, and subsequent cooling from, a 3D phase composed of "spheres", such as a body-centered cubic phase or a *Pm*$\bar{3}$*n* cubic phase, known also as Frank-Kasper A15. The directions of the reoriented columns preserve key interactions from the preceding cubic phase. However, SOM was observed so far in a very limited number of assemblies. The molecular determinants enabling SOM, and its generality, remain poorly understood. Here we report the synthesis and structural and retrostructural analysis of a perylene bisimide (PBI) with two self-assembling benzyl ether dendrons, 3,5-G2-PBI, and compare its assemblies with those of a previously reported PBI, 3,4,5-G2-PBI, which exhibits SOM and has an additional minidendritic building block in its dendrons. The removal of this minidendron in 3,5-G2-PBI eliminates its ability to self-assemble into supramolecular spheres and organize into a cubic phase, thereby precluding 3,5-G2-PBI from exhibiting SOM. This finding demonstrates hierarchical transfer of structural information from primary structure to material function, analogous to the misfolding of proteins into toxic structures such as those implicated in Alzheimer's and Prion diseases. The concepts exemplified here provide new insights into the hierarchical basis for SOM and will aid in the translation of the SOM concept to a broader diversity of soft matter such as block copolymers and surfactants.

Introduction

Memory – a sustained response to a transient stimulus[1] – is a fundamental biological phenomenon with applications in chemistry, materials science, and beyond. Its application in materials systems have realized a diverse range of functions, including shape memory polymers,[2–5] liquid crystal displays,[6,7] thermally responsive alloys[8,9] and ceramics.[10–12] In all of these examples, a transient stimulus, such as temperature or electric field, induces macroscopic changes with an associated function.

A memory effect on a supramolecular lengthscale was recently reported in two self-assembling dendrimers, one based on cyclotriveratrylene (CTV)[13] and another based on perylene bisimide (PBI).[14] Both of these dendrimers adopt crown conformations, or secondary structures,[13,15] which mediate the transition of their assemblies from supramolecular columns organized in a columnar hexagonal array, to supramolecular spheres organized in a cubic phase. Heating an oriented array of supramolecular columns into the cubic phase and subsequently cooling back into the columnar hexagonal phase provides otherwise inaccessible nanoscale architectures in which columnar domains are reoriented according to key directions in the preceding cubic phase. The directions of the cubic phase (the transient stimulus) are effectively impressed upon the orientations of the columnar domains (the sustained response). This memory effect, termed *supramolecular orientaional memory* (SOM),[13] has been observed for only a limited number of molecules[13,14] and relies on the preservation of structural information on the supramolecular level from the cubic phase to the columnar hexagonal phase.

SOM requires supramolecular assemblies which transition between a columnar phase and a 3D phase, organized from supramolecular spheres. Although this memory effect has so far been observed only in body-centered cubic (BCC, $Im\bar{3}m$)[14] and $Pm\bar{3}n$ cubic[13,16] (known also as Frank-Kasper A15[17,18] or Q_{223}[19]) phases organized from self-assembling dendrimers, SOM is expected to be transplanted to other 3D phases generated from spheres,[20] such as tetragonal ($P4_2/mnm$, known also as Frank-Kasper σ)[21] and 12-fold liquid quasicrystalline (LQC)[22,23] phases, comprising self-assembling dendrimers[24–28] and other soft matter,[29,30] including block copolymers[31–39] and surfactants.[40–42] These phases were originally

described for metallurgic systems and alloys,[43–45] but are also observed even in small molecules such as N_2,[46–51] CO,[50] and O_2,[52–55] raising the question of how generally SOM can be applied.

SOM is a function mediated by hierarchical organization from primary to quaternary structure.[56,57] Organization into relevant quaternary structures (both columnar and 3D sphere-based phases) relies on formation of appropriate tertiary structures (supramolecular columns and spheres, respectively), mediated by secondary structure (crown conformation), which is dictated by primary structure (molecular constitution). This clear hierarchical dependence on primary structure mirrors the generation of function in biological systems.[58,59] For example, Alzheimer's disease and Prion diseases associated with erroneous formation of β-sheets and their aggregation into toxic fibrils and prions.[60–65] The driving force for neither disease has been fully elucidated.

In this study we report the synthesis and structural analysis of a perylene bisimide (PBI) functionalized with two self-assembling dendrons, **(3,4Pr-3,5)12G2-0-PBI** (hereafter "**3,5-G2-PBI**", **1**), and compare its self-assembly with that of **(3,4Pr-3,4,5)12G2-0-PBI** (hereafter "**3,4,5-G2-PBI**", **2**), which was previously shown to exhibit SOM.[14] **3,5-G2-PBI** (**1**), which is related to **3,4,5-G2-PBI** (**2**) by removal of a single minidendritic branch from each dendron of **3,4,5-G2-PBI** (**2**). This modest change to the primary structure of the self-assembling PBI prevents formation of a supramolecular sphere, thus precluding **3,5-G2-PBI** (**1**) from exhibiting SOM. The elimination of function because of a structural change parallels the formation of disease-causing objects in Alzheimer's and Prion diseases, thus providing a synthetic model for protein misfolding.

Results and discussion

Fundamental crystallographic principles for SOM

SOM causes the reorientation of columnar hexagonal domains *via* heating to and subsequent cooling from a cubic phase for some molecules exhibiting both a columnar hexagonal and a cubic phase.[13,14] The orientation of the columnar domains, and therefore the nanoscale architecture that results from SOM, is dictated by directions of continuous columnar character in the preceding cubic phase. Fig. 1a–c depicts key directions in a columnar hexagonal, BCC, and $Pm\bar{3}n$ cubic lattice. In a hexagonal array of oriented

columns, the (001)-direction, denoted $[001]_{hex}$, runs alongs the column axis (Fig. 1a). The BCC lattice comprises one sphere at the corner of each cubic unit cell and a second sphere at the center of the cube (Fig. 1b). The (100)-direction runs along the edges of the cubic unit cell. Due to the symmetry of the cube, the (100)-direction is equivalent to the (010)- and (001)-directions, collectively denoted $[100]_{cub}$. Similarly, there are four equivalent body diagonals, denoted $[111]_{cub}$, which are arranged at 109.5° angles to each other,[66] akin to the tetrahedral arrangement of C–H bonds in methane. The sphere at the center of the BCC cell is in contact with the eight nearest neighbor spheres at the vertices, and hence there is continuous contact of supramolecular spheres along $[111]_{cub}$. This continuous contact leads to a distorted spherical shape.[67,68] The $Pm\bar{3}n$ cubic lattice not only contains the center and corner spheres of the BCC phase (compare yellow spheres in Fig. 1b and 1c), albeit no longer in close contact,[69] but also includes six spheres which lie on the faces of the cubic cell (Fig. 1c: red, orange, and blue distorted spheres). Each pair of face spheres has continuous columnar character along the (200)-direction, such that the "spheres" are substantially elongated along the (200)-direction,[69,70] which is parallel to the (100)-direction but bisects the face of the cubic unit cell.

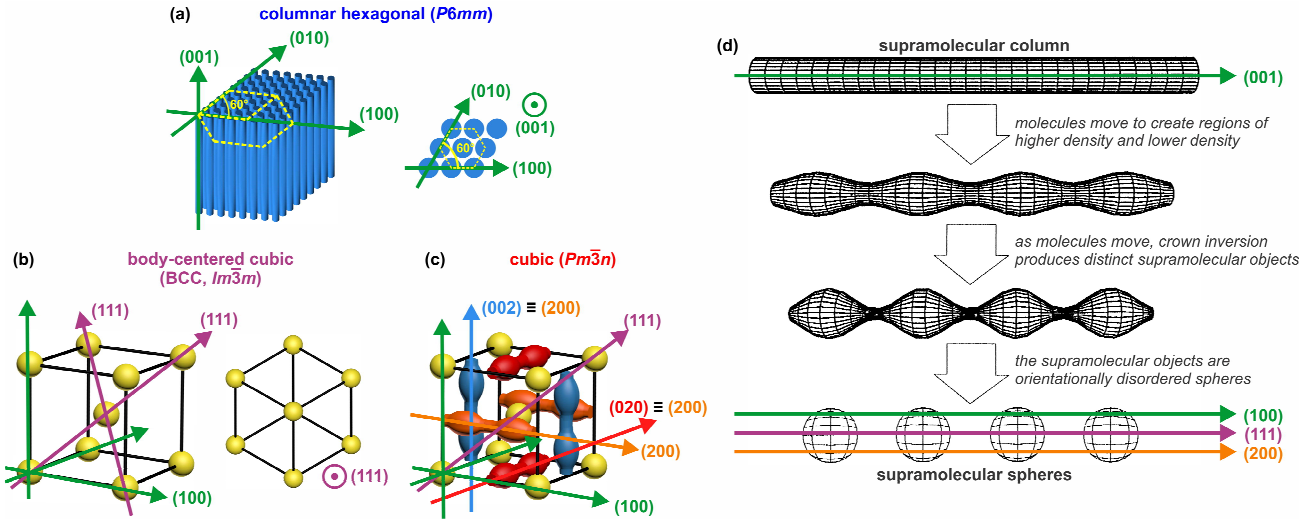

Figure 1. Summary of crystallographic concepts underpinning SOM. (a–c) Crystal structures and crystallographic directions in the (a) columnar hexagonal (*P6mm*) phase, (b) body-centered cubic (BCC, $Im\bar{3}m$) phase, and (c) cubic ($Pm\bar{3}n$) phase. (d) Schematic depiction of the "pinching off" model of sphere formation from supramolecular columns, adapted from ref. 71.

The transition between a columnar phase and a cubic phase requires a transition from supramolecular columns to supramolecular spheres. One possible mechanism for this process requires "pinching off"

columns to form spheres,[71] which involves movement of the self-assembling building blocks into regions of higher and lower density within the supramolecular column (Fig. 1d). This movement of molecules is mediated by their crown conformation and their ability to flip and form spherical objects.[13–15] When the supramolecular columns along $[001]_{hex}$ transform into supramolecular spheres, the direction in the cubic unit cell along which these spheres lie could be any direction, such as $[100]_{cub}$, $[111]_{cub}$, or $[200]_{cub}$.

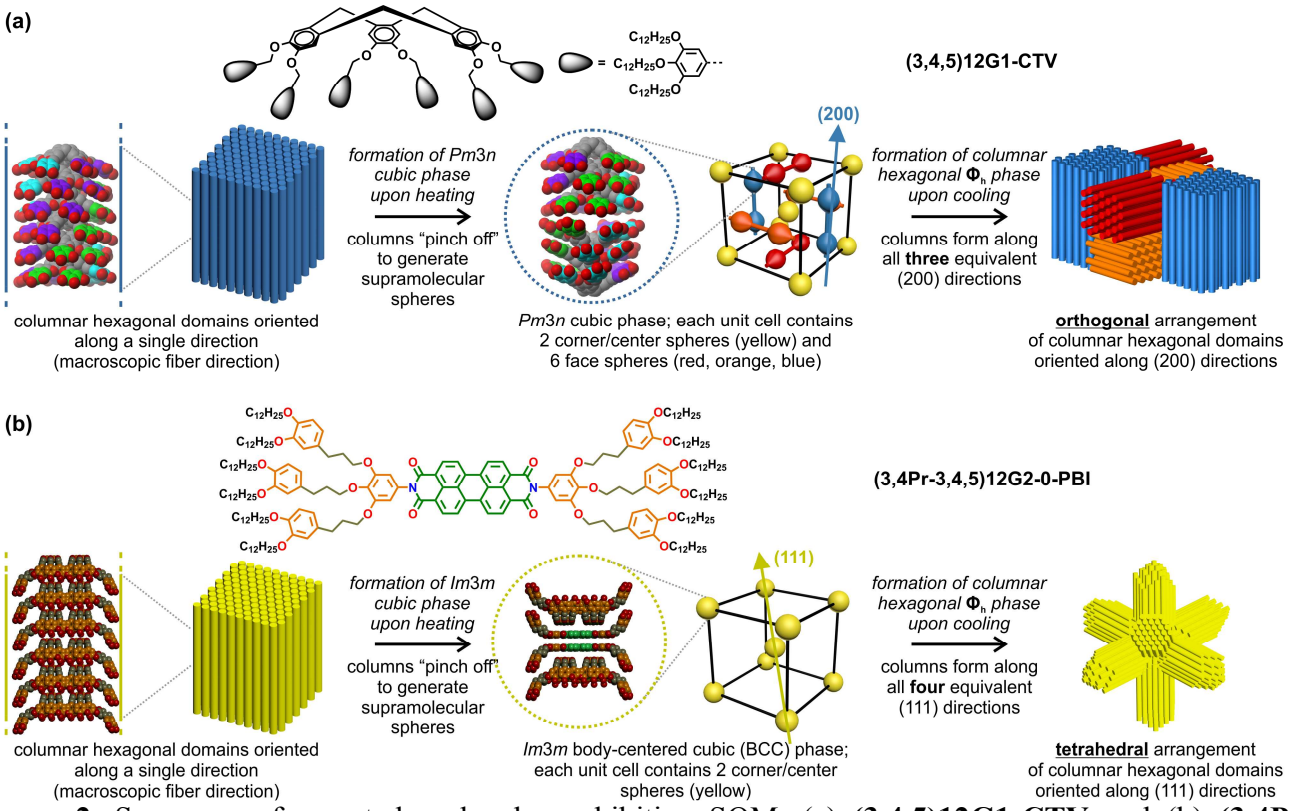

Figure 2. Summary of reported molecules exhibiting SOM. (a) **(3,4,5)12G1-CTV** and (b) **(3,4Pr-3,4,5)12G2-0-PBI** (**2**). Both molecules initially self-assemble into columnar hexagonal domains. Heating generates (a) a *Pm*$\bar{3}$*n* or (b) an *Im*$\bar{3}$*m* cubic phase in which there is continuous columnar character between spheres along the (a) (200) or (b) (111) directions. Cooling regenerates columnar hexagonal domains, oriented along the (a) three equivalent (200) directions or (b) four equivalent (111) directions of the preceding cubic phase, to give (a) an orthogonal or (b) a tetrahedral arrangement of supramolecular columns.

SOM was previously observed in two self-assembling dendrimers: one based on CTV, denoted **(3,4,5)12G1-CTV**[13] (Fig. 2a), and **3,4,5-G2-PBI** (**2**) (Fig. 2b).[14,15] **(3,4,5)12G1-CTV** self-assembled into a columnar hexagonal phase and, upon heating, a *Pm*$\bar{3}$*n* cubic phase (Fig. 2a). Upon transition from the oriented columnar phase to the *Pm*$\bar{3}$*n* cubic phase, the spheres which formed along $[001]_{hex}$ became the face spheres of the cubic unit cell, likely due to the continuous columnar character inherent in those

face spheres.[69,70] Upon cooling, this character was preserved along $[200]_{cub}$, and hence columnar domains were formed along all three (200)-directions to give an orthogonal arrangement of columnar domains (Fig. 2a, right). In contrast, **3,4,5-G2-PBI** (**2**) self-assembled into columnar hexagonal phases and a BCC phase.[15] The BCC phase is a special case of the hexagonal lattice[15] in which $[111]_{cub}$ is equivalent to $[001]_{hex}$ (Fig. 1b). Therefore the body diagonal of the BCC unit cell of **3,4,5-G2-PBI** (**2**) was oriented along the former column axis of the preceding columnar hexagonal phase. Upon cooling, all four $[111]_{cub}$ directions direct the formation of supramolecular columns to produce a tetrahedral arrangement of columnar hexagonal domains (Fig. 2b). Hence the arrangement of columnar domains in the hexagonal phase after cooling "remembers" – or, more accurately, preserves – directions of continuous columnar character in the cubic phase, such that different cubic phases give rise to different nanoscale architectures after cooling, driven by the directions of close contact between spheres in the cubic phase. A similar preservation of contact between notionally distinct supramolecular objects was recently invoked by Bates and coworkers to rationalize a form of "structural memory" in poly(isoprene)-*b*-poly(lactide) block copolymers.[39]

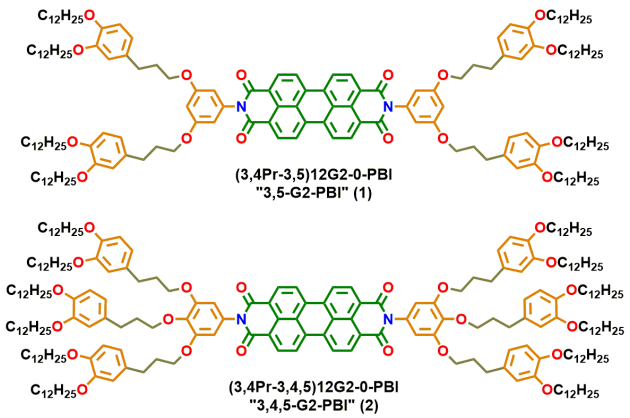

Scheme 1. Structures of (top) **(3,4Pr-3,5)12G2-0-PBI**, referred to as "**3,5-G2-PBI**" (**1**), and (bottom) **(3,4Pr-3,4,5)12G2-0-PBI**, referred to as "**3,4,5-G2-PBI**" (**2**).

Synthesis of perylene bisimides with second-generation self-assembling dendrons

To investigate the effect of primary structure on SOM, an analog of the SOM-exhibiting compound **3,4,5-G2-PBI** (**2**) was designed. **3,5-G2-PBI** (**1**) is also a PBI with two self-assembling dendrons, but lacks a minidendritic building block at the 4-position of both dendrons (Scheme 1). This structural

defect is analogous to biological molecules which may be damaged by oxidative cleavage or other degradation processes.

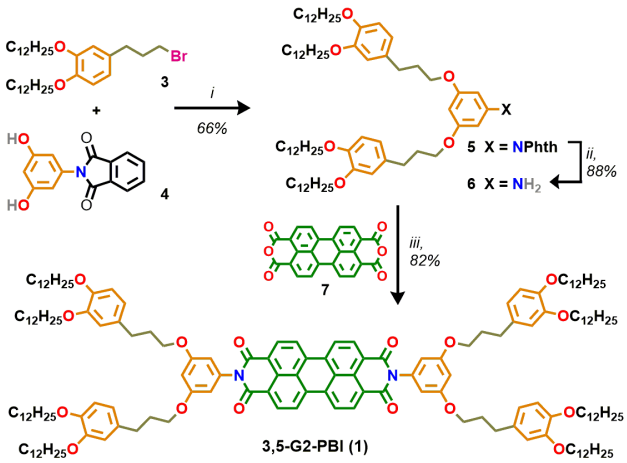

Scheme 2. Synthesis of **3,5-G2-PBI** (**1**). Reagents and conditions: (*i*) K_2CO_3, DMF, 75 °C, 16 h; (*ii*) $N_2H_4 \cdot H_2O$, EtOH/THF, reflux, 3 h; (*iii*) **7**, $Zn(OAc)_2 \cdot H_2O$, quinoline, 180 °C, 8 h.

Scheme 2 outlines the synthesis of **3,5-G2-PBI** (**1**). First generation propyl dendron bromide **3**, synthesized as reported,[72] was reacted with dihydroxyphthalimide **4**, also prepared according to reported procedures,[73] under Williamson esterification conditions with K_2CO_3 in DMF at 75 °C for 16 h, to give dendron phthalmide **5** in 66% yield after recrystallization from acetone. Deprotection of **5** with hydrazine hydrate in a refluxing mixture of EtOH and THF for 3 h gave unmasked dendron amine **6** in 88% yield after recrystallization (acetone). Imidization of commercially available perylene tetracarboxylic dianhydride (**7**) with the dendron amine **6** in quinoline at 180 °C for 8 h gave **3,5-G2-PBI** (**1**) as a red solid after chromatographic purification.

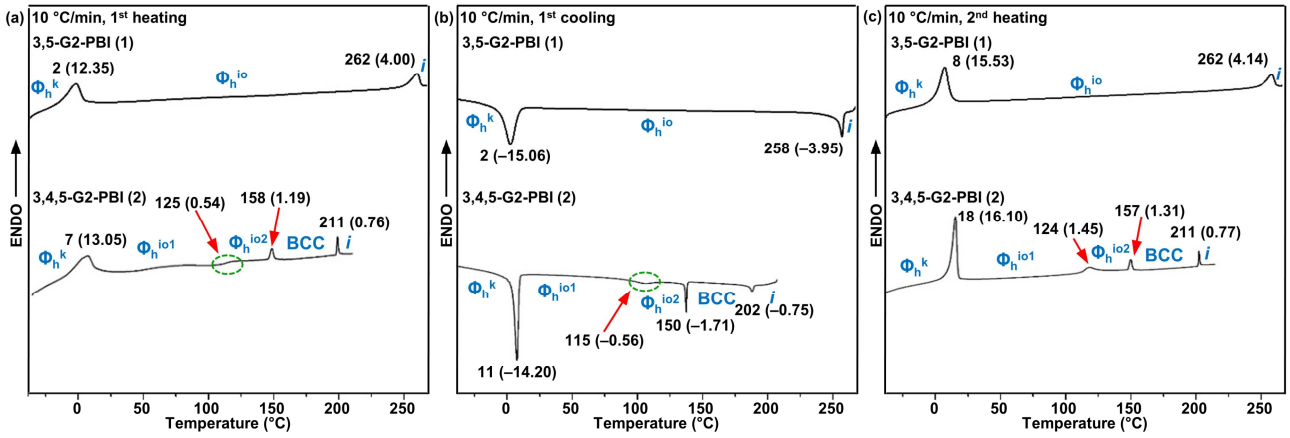

Figure 3. DSC traces of (top) **3,5-G2-PBI** (**1**) and (bottom) **3,4,5-G2-PBI** (**2**) recorded upon (a) first heating, (b) first cooling, and (c) second heating at a rate of 10 °C/min. Phases determined in XRD

(defined in main text), transition temperatures (in °C), and associated enthalpy changes (in parentheses, in kcal/mol) are indicated.

Thermal analysis by differential scanning calorimetry

The presence of first order phase transitions for **3,5-G2-PBI** (**1**) was analyzed by differential scanning calorimetry (DSC) at 10 °C/min (Fig. 3), and the identities of phases were identified by X-ray diffraction (XRD) experiments to be discussed later. A low temperature transition is observed at 2 °C on first heating and at 8 °C on second heating, corresponding to a transition between a columnar hexagonal crystalline ($\mathbf{\Phi_h^k}$) phase and a 2D columnar hexagonal phase with intracolumnar order ($\mathbf{\Phi_h^{io}}$). The $\mathbf{\Phi_h^{io}}$ phase exhibits a remarkably broad temperature range of thermal stability, ranging from 8 °C to 262 °C on second heating (Fig. 3c). At 262 °C there is a first order transition to the isotropic melt.

The existence of a single $\mathbf{\Phi_h^{io}}$ phase between 8 °C and the isotropization temperaure contrast the multiple phases exhibited by **3,4,5-G2-PBI** (**2**).[15] **3,4,5-G2-PBI** (**2**) self-assembles into two distinct $\mathbf{\Phi_h^{io}}$ phases, denoted $\mathbf{\Phi_h^{io1}}$ and $\mathbf{\Phi_h^{io2}}$, with a phase transition between them at 124 °C on second heating. Further heating above 157 °C generates a BCC phase, completely absent in **3,5-G2-PBI** (**1**), which transitions to an isotropic melt at 211 °C. The elimination of the cubic phase from **3,5-G2-PBI** (**1**) and concomitant stabilization of the $\mathbf{\Phi_h^{io}}$ phase are substantial changes resulting from the moderate structural defect of the missing minidendron at the 4-position.

Structural analysis of 3,5-G2-PBI (1) by X-ray diffraction and molecular modeling

The phases introduced in Fig. 3 were determined by XRD experiments coupled with iterative cycles of molecular modeling and simulation of the XRD arising from the proposed model. Experimental and simulated XRD of the $\mathbf{\Phi_h^k}$ phase of **3,5-G2-PBI** (**1**) are presented in Fig. 4 with a model consistent with the experimental XRD data. Diffraction features along the L = 0 layer line (Fig. 4a) indicate a hexagonal packing of supramolecular columns with diameter, D_{col}, of 42.1 Å, and the broad meridional feature on L = 4 suggests an intermolecular displacement, t, of 4.6 Å along the column axis, with the unit cell comprising four layers. The assignment of this phase as a crystalline phase is supported by the large enthalpy change associated with the transition between the $\mathbf{\Phi_h^{io}}$ and $\mathbf{\Phi_h^k}$ phases observed by DSC (Fig.

3a). The lack of off-axis *hkl* diffractions, which would be expected from a crystalline phase, is most likely attributable to a quenching in of the disorder of the Φ_h^{io} phase upon cooling, as seen previously for **3,4,5-G2-PBI** (**2**).[15]

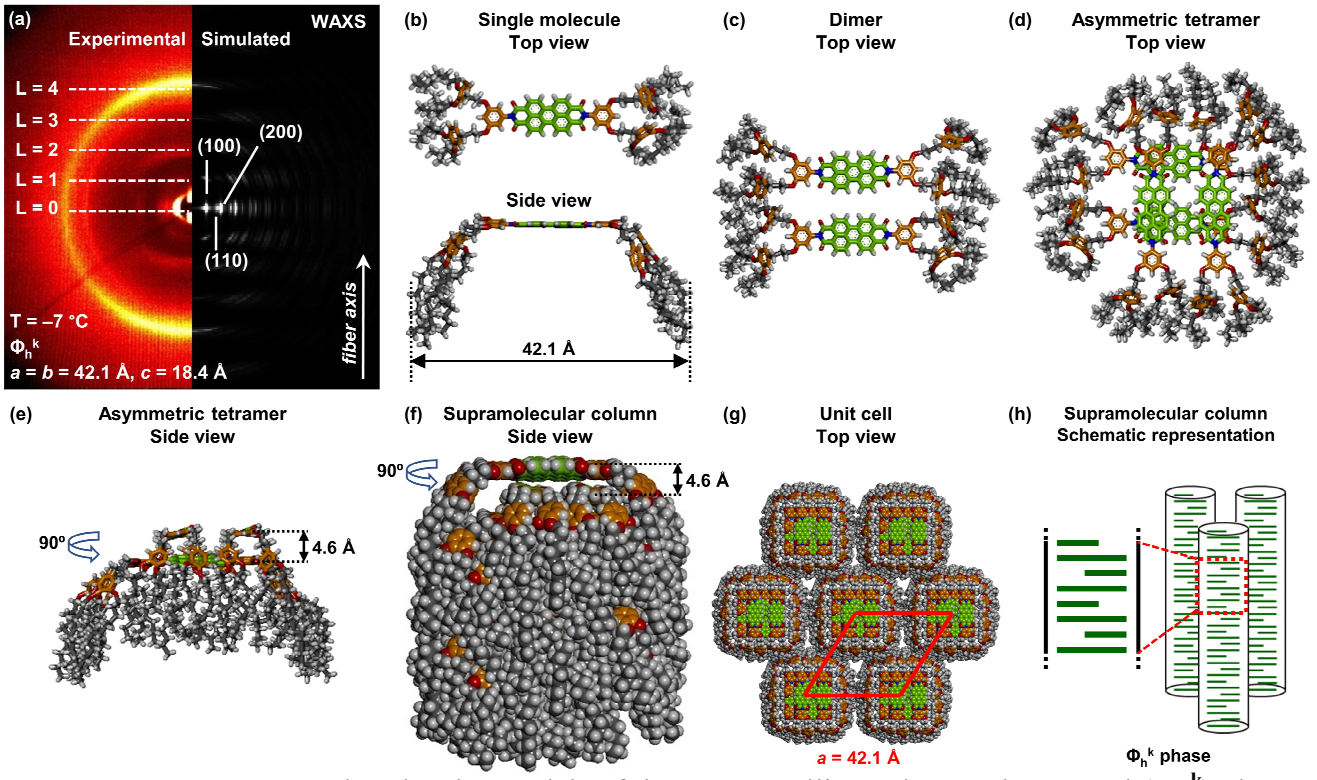

Figure 4. XRD patterns and molecular models of the 3D crystalline columnar hexagonal (Φ_h^k) phase of **3,5-G2-PBI** (**1**) generated from asymmetric tetrameric crowns. (a) Experimental X-ray diffraction pattern (left) compared with XRD pattern simulated from the model in (b–g) (right). Temperature, phase, lattice parameters, layer lines and fiber axis are indicated. (b–g) Molecular models of the Φ_h^k phase: (b) single molecule, top and side view; (c) dimer, top view; (d, e) asymmetric tetrameric crown, (d) top and (e) side view; (f) column, side view; (g) unit cell, top view. Color code: O, red; N, blue; C atoms of the PBI, green; C atoms of phenyl rings, orange; C atoms of the peripheral alkyl chains, gray; H, white. (h) Schematic representation of columns with molecules indicated as green bars.

The lattice parameters (D_{col} = 42.1 Å and t = 4.6 Å), taken with the measured density (ρ = 1.02 g/cm^3 at 23 °C) and molecular weight (M_{wt} = 2553.9 g/mol) can be used to calculate that there are ~1.7 molecules in each stratum of the supramolecular column (Table 1). Due to experimental uncertainty in both the density and XRD measurements, it can be concluded that there are about 2 dendronized PBI molecules per column stratum in the supramolecular columns of **3,5-G2-PBI** (**1**). Therefore, **3,5-G2-PBI** (**1**) (Fig. 4b) must form a dimeric column stratum (Fig. 4c). These dimers stack with an intermolecular distance of 4.6 Å to form an asymmetric tetramer (Fig. 4d, e), in which the two dimers are rotated by 90° but the center of the two constituent dimers is not colinear; that is, the dimers are offset. Stacking two

asymmetric tetramers (equivalently, four dimers) provides a single unit cell of the columnar hexagonal unit cell (Fig. 4f, g), with 8 molecules stacked as slightly offset dimers. A schematic representation for this packing is depicted in Fig. 4h.

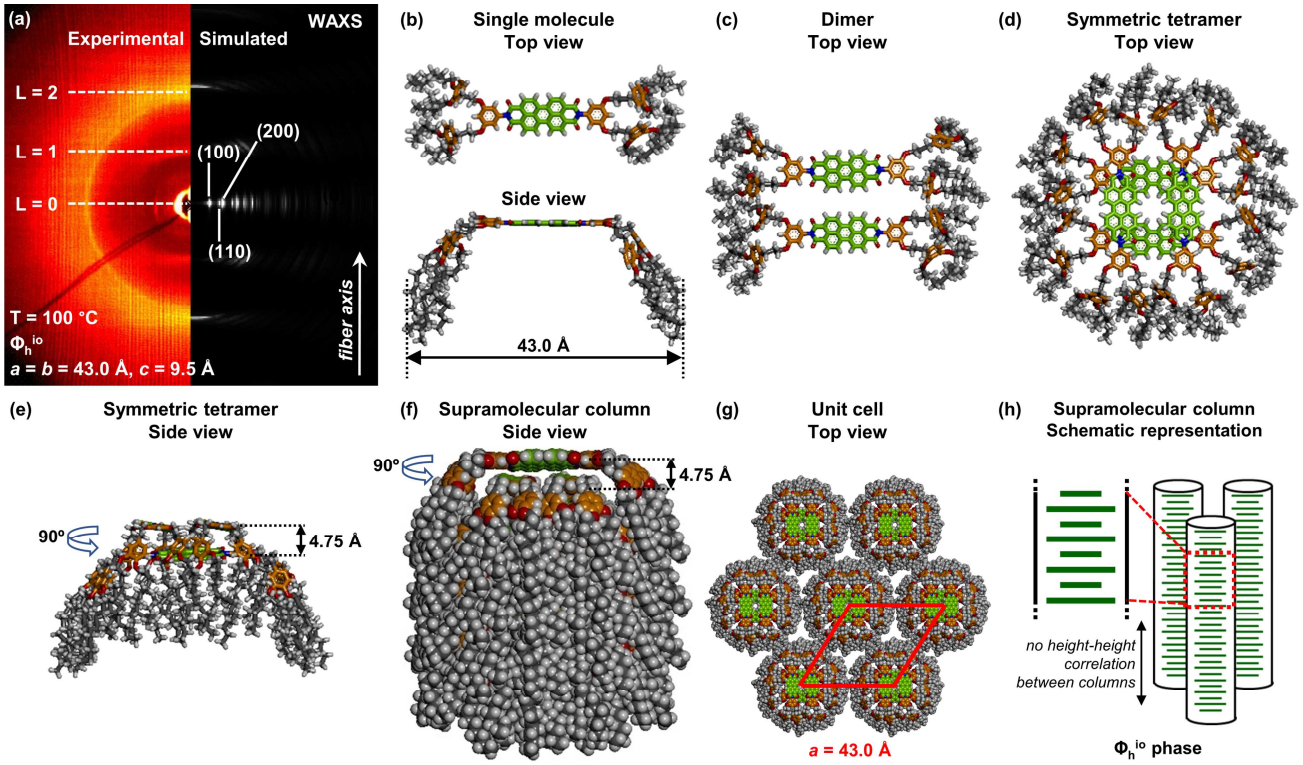

Figure 5. XRD patterns and molecular models of the 2D liquid crystalline columnar hexagonal phase with intracolumnar order (Φ_h^{io}) of **3,5-G2-PBI** (**1**) generated from symmetric tetrameric crowns. (a) Experimental X-ray diffraction pattern (left) compared with XRD pattern simulated from the model in (b–g) (right). Temperature, phase, lattice parameters, layer lines and fiber axis are indicated. (b–g) Molecular models of the Φ_h^{io} phase: (b) single molecule, top and side view; (c) dimer, top view; (d, e) asymmetric tetrameric crown, (d) top and (e) side view; (f) column, side view; (g) unit cell, top view. Color code: O, red; N, blue; C atoms of the PBI, green; C atoms of phenyl rings, orange; C atoms of the peripheral alkyl chains, gray; H, white. (h) Schematic representation of columns with molecules indicated as green bars.

The XRD pattern of **3,5-G2-PBI** (**1**) at 100 °C (Fig. 5a) and the large enthalpy change observed by DSC (Fig. 3a) is consistent with a columnar hexagonal phase with intracolumnar order, denoted Φ_h^{io}. In this phase, there is a regular arrangement of molecules within a supramolecular column, but there are no height-height correlations between the positions of molecules in adjacent columns. D_{col} of Φ_h^{io} is slightly larger than that of Φ_h^{k} (43.0 Å versus 42.1 Å), as is the intermolecular stacking along the column axis (t of Φ_h^{io} = 4.6 Å versus 4.75 Å for Φ_h^{k}). Calculation of the number of molecules per stratum yields a value of 1.9, and therefore it is again concluded that there are 2 molecules per column

stratum of the Φ_h^{io} phase. However, the presence of a broad meridional feature on L = 2 (Fig. 5a) suggests that there are only two layers per unit cell in the supramolecular column. Therefore, dimers of **3,5-G2-PBI** (**1**) (Fig. 5c) must assemble into symmetric tetramers (Fig. 5d, e). One symmetric tetramer constitutes the repeat unit of the supramolecular column, and therefore stacking of multiple tetramers describes the columns in the Φ_h^{io} phase (Fig. 5f–h).

Table 1. Structural Analysis of **3,5-G2-PBI** (**1**) by XRD

T (°C)	Phase [a]	*a*, *b*, *c* (Å) [b]	*t* (Å) [c]	ρ (g/cm^3) [d]	M_{wt} (g/mol) [e]	μ [f]	D_{col} (Å) [g]	d_{100}, d_{110}, d_{200}, d_{101} (Å)
–7	Φ_h^{k}	42.1, 42.1, 18.4	4.6	1.02	2553.9	1.7	42.1	36.6, 21.1, 18.2, 16.4
100	Φ_h^{io}	43.0, 43.0, 9.5	4.75			1.9	43.0	37.2, 21.5, 18.6, –

[a] Phase notation: Φ_h^{k} – 3D crystalline columnar hexagonal phase; Φ_h^{io} –2D liquid crystalline columnar hexagonal phase with intracolumnar order. [b] Lattice parameters calculated using $d_{hk} = (\sqrt{3}a/2)\cdot(h^2 + k^2 + hk)^{-1/2}$. [c] Average column stratum thickness calculated from the meridional axis features of WAXS fiber patterns. [d] Experimental density measured at 23 °C. [e] Molecular weight. [f] Average number of dendrimers forming the supramolecular column stratum with thickness *t*, calculated using $\mu = (N_A \cdot A \cdot t \cdot \rho)\cdot(M_{wt})^{-1}$ where $N_A = 6.022 \times 10^{23}$ mol^{-1} = Avogadro's number and *A* is the area of the column cross-section calculated from the lattice parameters. [g] Column diameter for Φ_h phases ($D_{col} = a$).

Self-assembly of 3,4,5-G2-PBI (2)

The self-assembly of **3,4,5-G2-PBI** (**2**) is reviewed in Fig. 6. The two lowest temperature phases formed by **3,4,5-G2-PBI** (**2**) are a Φ_h^{k} phase (below 18 °C, second heating) and Φ_h^{io1} phase (18 °C to 125 °C), which are very similar to the Φ_h^{k} and Φ_h^{io} phases exhibited by **3,5-G2-PBI** (**1**). The Φ_h^{k} phase of both PBIs comprises asymmetric tetramers stacked with a similar intermolecular distance (4.8 Å versus 4.6 Å). For both compounds, this Φ_h^{k} phase transforms upon heating into a Φ_h^{io} phase, at 8 °C for **3,5-G2-PBI** (**1**) and at 18 °C for **3,4,5-G2-PBI** (**2**) (Fig. 3c). The Φ_h^{io} phase of **3,5-G2-PBI** (**1**) (Fig. 5) and Φ_h^{io1} phase of **3,4,5-G2-PBI** (**2**) (Fig. 6) are constructed from symmetric tetramers stacked to form supramolecular columns with intracolumnar order but no height-height correlation between neighboring columns.

In contrast to **3,5-G2-PBI** (**1**), which forms only the isotropic melt upon heating from the Φ_h^{io} phase, **3,4,5-G2-PBI** (**2**) generates two additional phases. The first, observed from 124 °C to 157 °C (Fig. 3c), is another Φ_h^{io} phase, denoted Φ_h^{io2}. Upon transition from Φ_h^{io1} to Φ_h^{io2}, some molecules of **3,4,5-G2-PBI** (**2**) undergo crown inversion and form supramolecular spheres. However, these spheres maintain some orientational order along the column axis and therefore cannot rotate freely. The intrinsic

symmetry of **3,4,5-G2-PBI** (**2**) means that these molecules cannot form a perfectly isotropic sphere only by packing, and so the spheres in the columns of the Φ_h^{io2} phase are imperfect. Therefore, the structure is best conceived as a supramolecular column constructed from quasi-spherical supramolecular objects, similar to one of the intermediate structures depicted in Fig. 1d. Further heating of the Φ_h^{io2} phase provides, at 157 °C, a BCC phase. The quasi-spheres from the Φ_h^{io2} phase have complete orientational disorder, such that they appear, on average, spherical. Hence the oriented supramolecular columns of Φ_h^{io2} pinch off to form discrete supramolecular spheres in the BCC phase. The column direction of Φ_h^{io2}, $[100]_{hex}$, defines the body diagonal direction, $[111]_{cub}$, of the BCC phase, due to the hexagonal symmetry of the BCC phase (Fig. 1b).

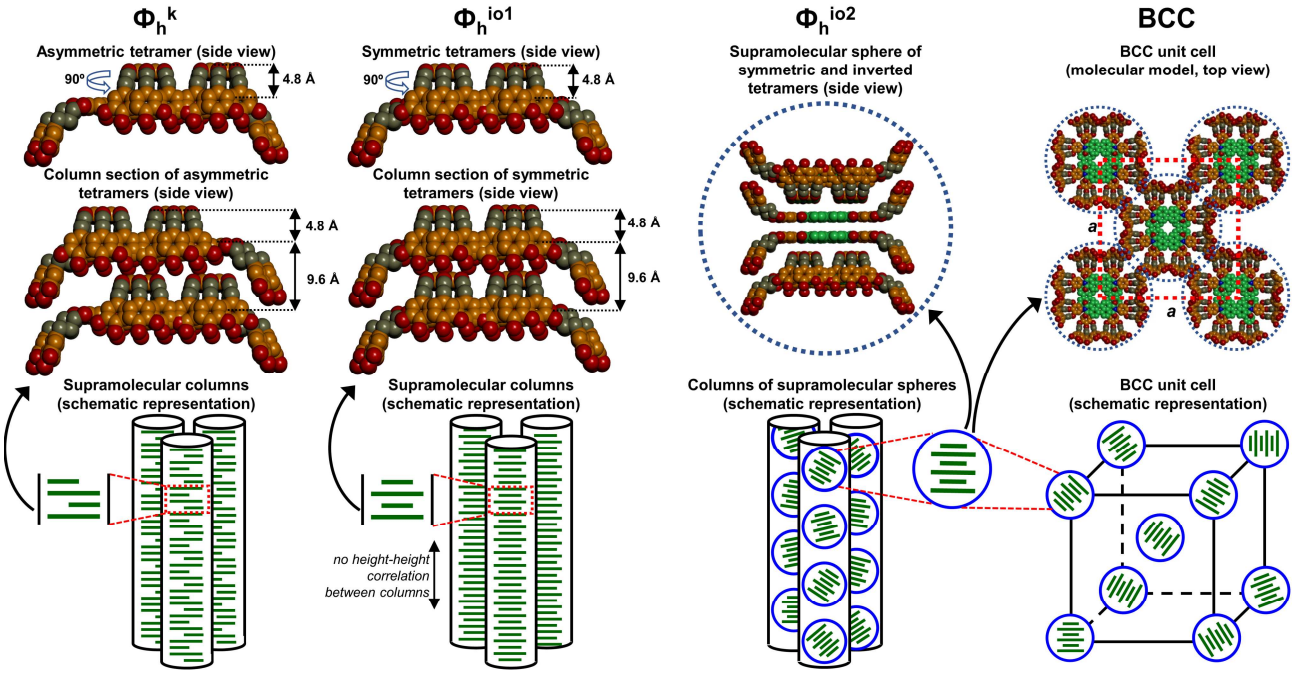

Figure 6. Schematic models of the four phases of **3,4,5-G2-PBI** (**2**). Phase notation: Φ_h^{k}, 3D crystalline columnar hexagonal phase; Φ_h^{io1}, low-temperature 2D liquid crystalline columnar hexagonal phase with intracolumnar order; Φ_h^{io2}, high-temperature 2D liquid crystalline columnar hexagonal phase with intracolumnar order, comprising columns of supramolecular; **BCC**, body-centered cubic periodic array generated from supramolecular spheres. Adapted from ref. [15].

Upon cooling the BCC phase of **3,4,5-G2-PBI** (**2**) below 150 °C (Fig. 3b), the supramolecular spheres lose their orientational freedom and generate supramolecular columns in Φ_h^{io2} along a body diagonal of the cubic unit cell, $[111]_{cub}$. All four (111)-directions are equivalent in the cubic unit cell, giving the supramolecualr columns of the Φ_h^{io2} phase an equal chance of being oriented along any one of these

four directions. Therefore, supramolecular columns orient along all four $[111]_{cub}$ directions, generating a tetrahedral arrangement of columnar hexagonal domains in the resultant Φ_h^{io2} phase (Fig. 2b). This arrangement persists upon cooling to the Φ_h^{io1} and Φ_h^{k} phases.

Losing SOM in assemblies of 3,5-G2-PBI (1)

The modest difference in the primary structures of **3,5-G2-PBI** (**1**) and **3,4,5-G2-PBI** (**2**) – the absence or presence of a minidendron at the 4-position of the second generation dendron – eliminates the ability of **3,5-G2-PBI** (**1**) to exhibit a material function, SOM. Molecular modeling was used to investigate the mechanism through which SOM is lost in assemblies of **3,5-G2-PBI** (**1**) (Fig. 7).

Both **3,4,5-G2-PBI** (**2**) and **3,5-G2-PBI** (**1**) self-assemble into supramolecular columns in which the dendrons are tilted towards the exterior of the column in a tapered conformation (Fig. 4b, 5b, and 6). As the assemblies are heated, the degree of motion and disorder increases in the self-assembling dendrons. For **3,4,5-G2-PBI** (**2**), this motion cannot be accommodated while maintaining the tapered conformation. Instead, the 3,4,5-dendron must adopt a conical conformation to reduce steric strain. This ability of a single building block to adopt multiple conformations during self-assembly is known as *quasi-equivalence*.[74,75] The conical conformation cannot be accommodated within the column, and drives formation of supramolecular spheres, first in the Φ_h^{io2} phase and subsequently in the BCC phase (Fig. 7a).

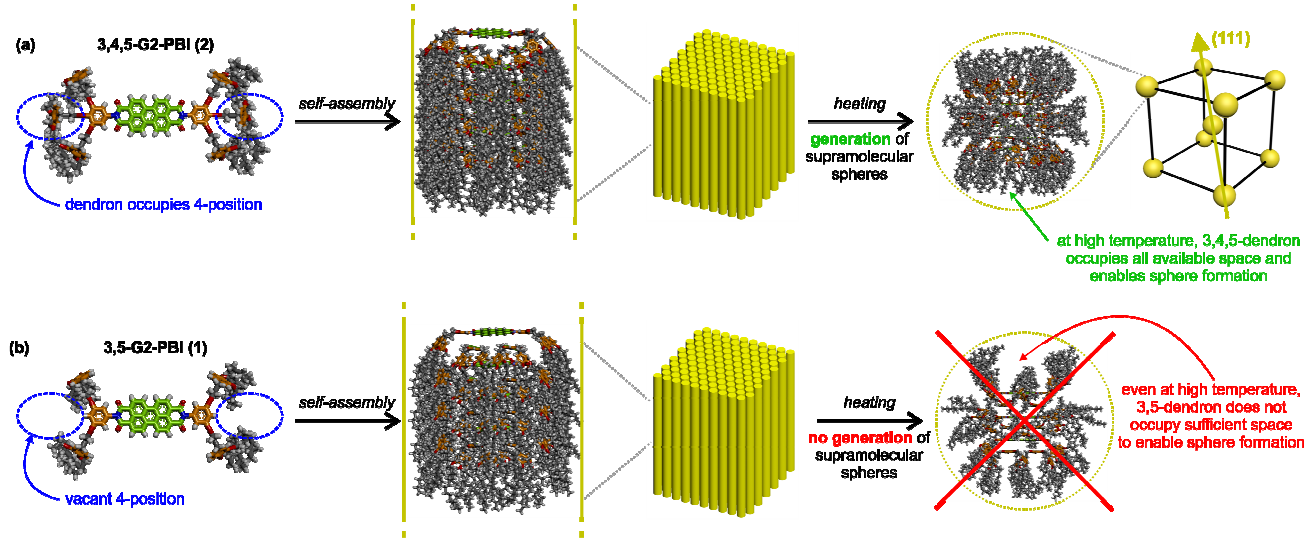

Figure 7. Comparison of supramolecular sphere formation by **3,4,5-G2-PBI** (**2**) and **3,5-G2-PBI** (**1**). (a) **3,4,5-G2-PBI** (**2**) self-assembles into supramolecular columns. However, at high temperature the

volume occupied by the 3,4,5-dendron increases and drives formation of a supramolecular sphere. (b) In contrast, the vacant 4-position in **3,5-G2-PBI** (**1**) accommodates the increased occupied volume of the dendrons at high temperature within the supramolecular column. A supramolecular sphere would have vacant space and thus its formation is disfavored.

In contrast, the vacant 4-position in the dendrons of **3,5-G2-PBI** (**1**) has two effects: it reduces the number of atoms which must be accommodated at the exterior of the column and also increases the available volume which the rest of the dendron can occupy. As the Φ_h^{io} phase of **3,5-G2-PBI** (**1**), the periphery of the column will undergo increased motion, but there remains sufficient space (Fig. 7a, b, broken blue ellipses) to accommodate the more disordered chains. Transition from a tapered conformation to a conical conformation is unnecessary. This effect has previously been observed for dendrons functionalized only in the 3- and 5-positions.[27,72] Molecular modeling (Fig. 7b, right) shows that even at high temperature, the 3,5-dendrons of **3,5-G2-PBI** (**1**) would be unable to sufficiently occupy the volume required to form a supramolecular sphere. Therefore, the columnar Φ_h^{io} phase of **3,5-G2-PBI** (**1**) persists until melting at 262 °C, which is not only beyond the transition temperature between Φ_h^{io2} and the BCC phase in **3,4,5-G2-PBI** (**1**) (157 °C), but also beyond the isotropization temperature of **3,4,5-G2-PBI** (**2**) (211 °C).

Conclusions

Modifying the primary structure of a self-assembling PBI, which displays SOM, **3,4,5-G2-PBI** (**2**), provides an analogous PBI, **3,5-G2-PBI** (**1**), which is unable to exhibit SOM in its assemblies. This elimination of the SOM function is mediated by a transfer of structural information through hierarchical self-assembly. With its modified primary structure, **3,5-G2-PBI** (**1**) adopts only a tapered conformation (secondary structure), without forming the conical conformation adopted by **3,4,5-G2-PBI** (**2**). The lack of a conical conformation precludes formation of a supramolecular sphere (tertiary structure) and eliminates subsequent organization into a BCC phase (quaternary structure). SOM requires a transition between a columnar phase and a 3D phase generated from spheres, and therefore SOM is not observed in assemblies of **3,5-G2-PBI** (**1**).

The mechanism by which SOM is eliminated in **3,5-G2-PBI** (**1**) is analogous to the elimination of healthy biological function in Alzheimer's and Prion diseases. The missing minidendritic building block at the 4-position of the dendrons in **3,5-G2-PBI** (**1**) compared to **3,4,5-G2-PBI** (**2**) can be viewed as a structural defect which alters its secondary structure. Defects or other changes to the secondary structure of a protein (or PBI) are transferred *via* hierarchical assembly to give misfolded tertiary and quaternary structures, and ultimately eliminate the desirable biological function or even generate additional detrimental function. In Prion diseases, the misfolded protein can disrupt the self-assembly of other, defect-free proteins. Investigations are ongoing to ascertain whether non-SOM molecules can disrupt the memory effect of SOM molecules, or, conversely, whether molecules capable of exhibiting SOM can induce a structurally defective molecule to exhibit desirable function.

The PBIs reported here provide a clear demonstration of the effect of changes to the primary structure on the generation of function *via* hierarchical self-assembly. This work also further enhances our understanding of SOM, but also raises some additional questions. Both **(3,4,5)12G1-CTV**[13] (Fig. 2a) and **3,4,5-G2-PBI** (**2**) adopt crown conformations in their supramolecular columns and spheres. Is a crown conformation sufficient to exhibit SOM? Will other crown-like CTV derivatives[76] exhibit SOM? How about other self-assembling dendrimers which adopt crown conformations, such as triphenylenes?[77] Of relevance to other soft matter, such as block copolymers and surfactants, is whether a crown conformation is required, or whether conical molecules[78] or micellar structures can also exhibit SOM? How about spheres made from a single dendron or polymer chain?[79] These questions are under active investigation and are expected to provide additional hints at how this concept can be generalized to the diverse range of building blocks, including block copolymers and surfactants, which self-organize into 3D phases comprising supramolecular spheres.

Experimental

Materials

Hydrazine hydrate ($N_2H_4 \cdot H_2O$), zinc acetate dihydrate ($Zn(OAc)_2 \cdot 2H_2O$), and quinoline (all from Acros), Potassium carbonate (K_2CO_3) (from Alfa Aesar), and DMF, EtOH, and THF (all from Fisher, ACS reagent) were used as received. 3-[(3,4-Bis(dodecyl-1-oxy)phenyl]propyl bromide[72] (**3**) and 2-(3,5-

dihydroxyphenyl)isoindole-1,3-dione[73] (**4**) were synthesized according to previously reported procedures.

Techniques

The purity, and the structural identity of the intermediary and final products were assessed by a combination of techniques that includes thin-layer chromatography (TLC), high pressure liquid chromatography (HPLC), ^{1}H and ^{13}C NMR, and matrix-assisted laser desorption/ionization time-of-flight (MALDI-TOF) mass spectrometry.

High Pressure Liquid Chromatography (HPLC). High pressure liquid chromatography (HPLC) was carried out using Shimadzu LC-20AD high-performance liquid chromatograph pump, a PE Nelson Analytical 900 Series integration data station, a Shimadzu RID-10A refractive index (RI) detector, and three AM gel columns (a guard column, 500 Å, 10 μm, and 104 Å, 10 μm). THF was used as solvent at an oven temperature of 40 °C. UV absorbance at 254 nm was used as detector.

Solution NMR. ^{1}H NMR (500 MHz), and ^{13}C NMR (126 MHz) spectra were recorded on a Bruker DRX 500 instrument using the solvent indicated at 300 K.

Matrix-Assisted Laser Desorption/Ionization Time of Flight (MALDI-TOF). MALDI-TOF mass spectrometry was performed on PerSeptive Biosystems-Voyager-DE (Framingham, MA) mass spectrometer equipped with a nitrogen laser (337 μm), and operating in linear mode. Internal calibration was performed using Angiotensin II, and Bombesin as standards. The analytical samples were obtained by mixing THF solution of the sample (5–10 mg/mL), and the matrix (3,5-dihydroxybenzoic acid) (10 mg/mL) in a 1:1 to 1:5 v/v ratio. The prepared solution (0.5 μL) was loaded on the MALDI plate, and allowed to dry at 25 °C before the plate was inserted into the vacuum chamber of the MALDI instrument. The laser steps, and voltages were adjusted depending on the molecular weight, and the nature of each analyte.

Differential Scanning Calorimetry (DSC). Thermal transitions were measured on TA Q100 differential scanning calorimeter integrated with a refrigerated cooling system (RCS). The transition temperatures were measured as the maxima and minima of their endothermic and exothermic peaks, respectively. Indium and sapphire were used as calibration standards.

X-ray Diffraction (XRD). XRD measurements were performed using Cu-$K_{\alpha 1}$ radiation (λ = 1.542 Å) from a Bruker-Nonius FR-591 rotating anode X-ray source equipped with a 0.2 × 0.2 mm^2 filament and operated at 3.4 kW. Osmic Max-Flux optics, and triple pinhole collimation were used to obtain a highly collimated beam with a 0.3 × 0.3 mm^2 spot on a Bruker-AXS Hi-Star multiwire area detector. To minimize attenuation, and background scattering, an integral vacuum was maintained along the length of the flight tube, and within the sample chamber. Samples were held in glass capillaries (1.0 mm in diameter), mounted in a temperature-controlled oven (temperature precision: ± 0.1 °C, temperature

range from –10 °C to 210 °C). Aligned samples for fiber XRD experiments were prepared using a custom-made extrusion device.[80] The powdered sample (~10 mg) was extruded in the liquid crystal phase. Typically, the aligned samples have a thickness of 0.3–0.7 mm, and a length of 3–7 mm. All XRD measurements were done with the aligned sample axis perpendicular to the beam direction. Primary XRD analysis was performed using Datasqueeze (version 3.0.5).

Molecular Modelling and Simulation. Molecular modeling, and simulation experiments were performed using Materials Studio (version 5) software from Accelrys. The Forcite module was used to perform the energy minimizations on the supramolecular structures.

Density Measurements. For density measurements, a small mass of sample (~0.4 mg) was placed in a vial filled with water followed by ultrasonication to remove the air bubbles embedded within the sample. The sample sank to the bottom of the vial due to its high density compared with water. A saturated aqueous solution of potassium iodide (KI) was then added into the solution at ~0.1 g per aliquot to gradually increase the solution density. KI was added at an interval of at least 20 min to ensure equilibrium within the solution. When the sample was suspended in the middle of the solution, the density of the sample was identical to that of the solution, which was measured by a 10 mL volumetric flask.

Synthesis of 3,5-G2-PBI (1)

*2-{3,5-Bis-[3-(3,4-bis(dodecyl-1-oxy)phenyl)propoxy]phenyl}isoindole-1,3-dione (**5**).* In a 100 mL three-necked flask equipped with a condenser were placed *N*,*N*-dimethylformamide (DMF, 30 mL) together with dry K_2CO_3 (0.5 g, 3.5 mmol). The resulting suspension was degassed with a stream of Ar for 15 min. 2-(3,5-Dihydroxyphenyl)isoindole-1,3-dione (**4**) (0.20 g, 0.78 mmol) and 3-[(3,4-bis(dodecyl-1-oxy)phenyl]propylbromide (**3**) (0.90 g, 1.59 mmol) were added, and the mixture was stirred and heated at 75 ºC for 1 6h. The reaction mixture was poured into cold water (50 mL) and the resulting precipitate was filtered, washed with water and methanol and dried. Recrystallization from acetone produced 0.6 g (66 %) of white crystals. Purity (HPLC): 99%+, TLC (SiO_2, CH_2Cl_2): R_f = 0.65. ^{1}H NMR ($CDCl_3$, δ, ppm, TMS): 0.89 (t, J = 6.4 Hz, 12H, 4CH_3), 1.28 (m, 64H, 4$CH_3(CH_2)_8$), 1.46 (m, 8H, 4AlkC$H_2$$CH_2CH_2OAr$), 1.79 (m, 8H, 4Alk$CH_2CH_2$$CH_2OAr$), 1.95 (m, 4H, 2Ar$CH_2CH_2$$CH_2OAr$), 2.65 (t, J = 5.7 Hz, 4H, 2ArC$H_2$$CH_2CH_2OAr$), 3.94–4.02 (overlapped m, 12H, 4Alk$CH_2CH_2CH_2OAr$ and 2Ar$CH_2CH_2CH_2OAr$), 6.12 (s, 1H, Ar*H*, para to $N(C=O)_2$), 6.72–6.81 (overlapped m, Ar*H*, *ortho* and *meta* to OAlk), 6.91 (s, 2H, Ar*H ortho* to $N(C=O)_2$), 7.73 (dd, J = 8.3, 2.1 Hz, 2H, Ar*H meta* to C=O), 8.20 (dd, J = 8.3, 2.1 Hz, 2H, Ar*H ortho* to C=O). ^{13}C NMR ($CDCl_3$, δ, ppm, TMS): 14.5 (CH_3), 23.1 (CH_2CH_3), 26.5 ($CH_2CH_2CH_2OAr$), 29.7 ($CH_3(CH_3)_2CH_2$), 30.0–30.1 (overlapped $CH_3(CH_2)_3(CH_2)_5$), 30.7 (CH_2CH_2OAr), 32.4 (Ar$CH_2CH_2CH_2OAr$, 3,5 positions), 32.8 (Ar$CH_2CH_2CH_2OAr$, 3,5 positions), 71.7 (Ar$CH_2CH_2CH_2OAr$, 3,5 positions), 73.7 (AlkCH_2OAr), 97.8

(Ar*C para* to N(C=O)$_2$), 98.9 (Ar*C ortho* to N(C=O)$_2$), 114.6 (Ar*C* (2') *ortho* to $CH_2CH_2CH_2OAr$, 3,5 positions), 114.9 (Ar*C* (3') *meta* to $CH_2CH_2CH_2OAr$, 3,5 positions), 120.7 (Ar*C* (6') *ortho* to $CH_2CH_2CH_2OAr$, 3,5 positions), 127.4 (Ar*C ortho* to (C=O)$_2$), 132.1 (Ar*C meta* to C=O), 132.7 (Ar*C* ipso to C=O), 140.1 (Ar*C* ipso to N(C=O)$_2$), 159.6 (Ar*C* ipso to $ArCH_2CH_2CH_2O$), 164.5 (*C*=O).

*3,5-Bis-[3-(3,4-bis(dodecyl-1-oxy)phenyl)propoxy]phenylamine (**6**).* To a solution of dendron phthalimide **5** (0.53 g, 0.43 mmol) in a mixture of EtOH (5 mL) and THF (15 mL) was added hydrazine monohydrate ($N_2H_4.H_2O$) (0.11 g, 2.2 mmol). The reaction mixture was refluxed under Ar atmosphere for 3 h. The solvents were removed under reduced pressure and the resulting residue was dissolved in minimal volume of CH_2Cl_2 and passed through a short column of silica gel using CH_2Cl_2/acetone (10:1 v/v) as eluent. The solvents were fully evaporated and the remaining product was recrystallized from acetone to produce 0.42 g (88 %) of pure product as white crystals. Purity (HPLC): 99%+, TLC (SiO_2, CH_2Cl_2/acetone 10:1): R_f = 0.45. ^{1}H NMR ($CDCl_3$, δ, ppm, TMS): 0.89 (t, *J* = 6.4 Hz, 12H, 4C*H*$_3$), 1.28 (m, 64H, 4CH$_3$(C*H*$_2$)$_8$), 1.46 (m, 8H, 4AlkC*H*$_2$CH$_2$CH$_2$OAr), 1.79 (m, 8H, 4AlkCH$_2$C*H*$_2$CH$_2$OAr), 1.95 (m, 4H, 2ArCH$_2$C*H*$_2$CH$_2$OAr), 2.65 (t, *J* = 5.7 Hz, 4H, 2ArC*H*$_2$CH$_2$CH$_2$OAr), 3.94-4.02 (overlapped m, 12H, 4AlkCH$_2$CH$_2$C*H*$_2$OAr and ArCH$_2$CH$_2$C*H*$_2$OAr), 5.85 (s, 2H, ArH *ortho* to NH$_2$), 5.90 (s, 1H, Ar*H*, *para* to NH$_2$), 6.72–6.81 (overlapped m, 6H, Ar*H*, *ortho* and *meta* to OAlk). ^{13}C NMR ($CDCl_3$, δ, ppm, TMS): 14.5 (*C*H$_3$), 23.1 (*C*H$_2$CH$_3$), 26.5 (*C*H$_2$CH$_2$CH$_2$OAr), 29.7 (CH$_3$(CH$_3$)$_2$*C*H$_2$), 30.0–30.1 (overlapped CH$_3$(CH$_2$)$_3$(*C*H$_2$)$_5$), 30.6 (*C*H$_2$CH$_2$OAr), 32.5 (ArCH$_2$CH$_2$CH$_2$OAr, 3,5 positions), 32.9 (ArCH$_2$*C*H$_2$CH$_2$OAr, 3,5 positions), 71.5 (ArCH$_2$CH$_2$*C*H$_2$OAr, 3,5 positions), 73.2 (Alk*C*H$_2$OAr), 92.5 (Ar*C para* to NH$_2$), 95.9 (Ar*C ortho* to NH$_2$), 114.6 (Ar*C* (2') *ortho* to $CH_2CH_2CH_2OAr$, 3,5 positions), 114.9 (Ar*C* (3') *meta* to $CH_2CH_2CH_2OAr$, 3,5 positions), 120.7 (Ar*C* (6') *ortho* to $CH_2CH_2CH_2OAr$, 3,5 positions), 147.1 (Ar*C* ipso to NH$_2$), 159.9 (Ar*C* ipso to $ArCH_2CH_2CH_2O$).

*(3,4Pr-3,5)12G1-0-PBI (**3,5-G2-PBI**, **2**).* A suspension of perylene tetracarboxylic dianhydride (**7**) (71 mg, 0.18 mmol), dendron amine **6** (0.4 g, 0.37 mmol) and Zn(OAc)$_2$·2H$_2$O (40 mg, 0.18 mmol) in quinoline (7 mL) was stirred at 180 ºC under Ar atmosphere for 8 h. The reaction mixture was allowed to cool to 23 °C whereupon it was poured into HCl (1 M, 20 mL). The resulting precipitate was filtered, washed with water (20 mL) and methanol (20 mL), and dried. The crude product was purified by silica gel column chromatography using CH_2Cl_2/acetone (20:1, v/v). The resulting red powder was dissolved in CH_2Cl_2 and precipitated by the addition of methanol to produce 0.38 g (82 %) as a red solid. TLC (SiO_2, CH_2Cl_2/acetone 20:1): R_f = 0.42. Purity (HPLC): 99%+. ^{1}H NMR ($CDCl_3$, δ, ppm, TMS): 0.89 (t, *J* = 6.4 Hz, 24H, 8C*H*$_3$), 1.28 (m, 128H, 8CH$_3$(C*H*$_2$)$_8$), 1.47 (m, 16H, 8AlkC*H*$_2$CH$_2$CH$_2$OAr), 1.79 (m, 16H, 8AlkCH$_2$C*H*$_2$CH$_2$OAr), 2.08 (m, 8H, 4ArCH$_2$C*H*$_2$CH$_2$OAr), 2.73 (t, *J* = 5.7 Hz, 8H, 4ArC*H*$_2$CH$_2$CH$_2$OAr), 3.96–4.00 (overlapped m, 24H, 8AlkCH$_2$CH$_2$CH$_2$OAr and 4ArC*H*$_2$CH$_2$CH$_2$OAr), 6.54 (s, 2H, Ar*H ortho* to $ArCH_2CH_2CH_2O$), 6.62–6.81 (overlapped m, 12H,

Ar*H*, *ortho* and *meta* to OAlk), 6.82 (s, 4H, Ar*H*, *ortho* to $N(C=O)_2$), 8.63 (d, *J* = 8.1 Hz, 4H, H2,5,8,11), 8.74 (d, *J* = 8.1 Hz, 4H, H1,6,7,12). ^{13}C NMR ($CDCl_3$, δ, ppm, TMS): 14.5 (CH_3), 23.2 (CH_2CH_3), 26.5 ($CH_2CH_2CH_2OAr$), 29.9 ($CH_3(CH_3)_2CH_2$), 30.1-30.3 ($CH_3(CH_2)_3(CH_2)_5$), 30.7 (CH_2CH_2OAr), 32.8 ($ArCH_2CH_2CH_2OAr$, 3,5 positions), 32.9 ($ArCH_2CH_2CH_2OAr$, 3,5 positions), 71.5 ($ArCH_2CH_2CH_2OAr$, 3,5 positions), 73.2 ($AlkCH_2OAr$), 101.2 (Ar*C para* to $N(C=O)_2$), 106.5 (Ar*C ortho* to $N(CO)_2$), 114.5 (Ar*C* (2') *ortho* to $CH_2CH_2CH_2OAr$, 3,5 positions), 114.7 (Ar*C* (3') *meta* to $CH_2CH_2CH_2OAr$, 3,5 positions), 120.9 (Ar*C* (6') *ortho* to $CH_2CH_2CH_2OAr$, 3,5 positions), the signals at 122.4, 123.1, 125.7, 128.7, 130.9 and 131.2, correspond to perylene carbons; 141.2 (Ar*C* ipso to $N(C=O)_2$), 159.9 (Ar*C* ipso to $ArCH_2CH_2CH_2O$), 162.3 (*C*=O).

Conflicts of interest

There are no conflicts of interest to declare.

Acknowledgements

Financial support by the National Science Foundation (DMR-1066116 (VP) and DMR-1120901 (VP and MLK)), the Humboldt Foundation (VP) and the P. Roy Vagelos Chair at Penn (VP) is gratefully acknowledged. MLK thanks HH Sheikh Saud for financial support *via* a Sheikh Saqr Research Fellowship. BEP thanks the Howard Hughes Medical Institute for an International Student Research Fellowship. The authors thank Professor Paul A. Heiney from Penn for useful discussions.

References

1 D. R. Burrill and P. A. Silver, *Cell*, 2010, **140**, 13–18.

2 A. Lendlein and R. Langer, *Science*, 2002, **296**, 1673–1676.

3 A. Lendlein, H. Jiang, O. Junger and R. Langer, *Nature*, 2005, **434**, 879–882.

4 W. Sokolowski, A. Metcalfe, S. Hayashi, L. Yahia and J. Raymond, *Biomed. Mater.*, 2007, **2**, S23–S27.

5 A. A. Shah, B. Schultz, W. Zhang, S. C. Glotzer and M. J. Solomon, *Nat. Mater.*, 2014, **14**, 117–124.

6 I. Dozov, M. Nobili and G. Durand, *Appl. Phys. Lett.*, 1997, **70**, 1179–1181.

7 F. Serra, M. Buscaglia and T. Bellini, *Mater. Today*, 2011, **14**, 488–494.

8 A. Ölander, *J. Am. Chem. Soc.*, 1932, **54**, 3819–3833.

9 H. R. Wenk, P. Kaercher, W. Kanitpanyacharoen, E. Zepeda-Alarcon and Y. Wang, *Phys. Rev. Lett.*, 2013, **111**, 1–5.

10 K. E. Schurch and K. H. G. Ashbee, *Nature*, 1977, **266**, 706–707.

11 M. V. Swain, *Nature*, 1986, **322**, 234–236.

12 A. Lai, Z. Du, C. L. Gan and C. A. Schuh, *Science*, 2013, **341**, 1505–1508.

13 M. Peterca, M. R. Imam, S. D. Hudson, B. E. Partridge, D. Sahoo, P. A. Heiney, M. L. Klein and V. Percec, *ACS Nano*, 2016, **10**, 10480–10488.

14 D. Sahoo, M. Peterca, E. Aqad, B. E. Partridge, P. A. Heiney, R. Graf, H. W. Spiess, X. Zeng and

V. Percec, *ACS Nano*, 2017, **11**, 983–991.

15 D. Sahoo, M. Peterca, E. Aqad, B. E. Partridge, P. A. Heiney, R. Graf, H. W. Spiess, X. Zeng and V. Percec, *J. Am. Chem. Soc.*, 2016, **138**, 14798–14807.

16 S. D. Hudson, H.-T. Jung, V. Percec, W.-D. Cho, G. Johansson, G. Ungar and V. S. K. Balagurusamy, *Science*, 1997, **278**, 449–452.

17 A. K. Sinha, *Prog. Mater. Sci.*, 1972, **15**, 81–185.

18 G. Ungar and X. Zeng, *Soft Matter*, 2005, **1**, 95–106.

19 P. Mariani, V. Luzzati and H. Delacroix, *J. Mol. Biol.*, 1988, **204**, 165–189.

20 M. Huang, K. Yue, J. Wang, C. H. Hsu, L. Wang and S. Z. D. Cheng, *Sci. China Chem.*, 2017, **61**, 33–45.

21 G. Ungar, Y. Liu, X. Zeng, V. Percec and W.-D. Cho, *Science*, 2003, **299**, 1208–1211.

22 X. Zeng, G. Ungar, Y. Liu, V. Percec, A. E. Dulcey and J. K. Hobbs, *Nature*, 2004, **428**, 157–160.

23 T. Dotera, *Isr. J. Chem.*, 2011, **51**, 1197–1205.

24 V. Percec, W.-D. Cho, P. E. Mosier, G. Ungar and D. J. P. Yeardley, *J. Am. Chem. Soc.*, 1998, **120**, 11061–11070.

25 V. Percec, W. D. Cho and G. Ungar, *J. Am. Chem. Soc.*, 2000, **122**, 10273–10281.

26 V. Percec, W.-D. Cho, G. Ungar and D. J. P. Yeardley, *J. Am. Chem. Soc.*, 2001, **123**, 1302–1315.

27 V. Percec, C. M. Mitchell, W. D. Cho, S. Uchida, M. Glodde, G. Ungar, X. Zeng, Y. Liu, V. S. K. Balagurusamy and P. A. Heiney, *J. Am. Chem. Soc.*, 2004, **126**, 6078–6094.

28 V. Percec, M. N. Holerca, S. Nummelin, J. J. Morrison, M. Glodde, J. Smidrkal, M. Peterca, B. M. Rosen, S. Uchida, V. S. K. Balagurusamy, M. J. Sienkowska and P. A. Heiney, *Chem. Eur. J.*, 2006, **12**, 6216–6241.

29 X. Feng, R. Zhang, Y. Li, Y. L. Hong, D. Guo, K. Lang, K. Y. Wu, M. Huang, J. Mao, C. Wesdemiotis, Y. Nishiyama, W. Zhang, T. Miyoshi, T. Li and S. Z. D. Cheng, *ACS Cent. Sci.*, 2017, **3**, 860–867.

30 W. Zhang, X. Lu, J. Mao, C. H. Hsu, G. Mu, M. Huang, Q. Guo, H. Liu, C. Wesdemiotis, T. Li, W. Bin Zhang, Y. Li and S. Z. D. Cheng, *Angew. Chem. Int. Ed.*, 2017, **56**, 15014–15019.

31 F. S. Bates and G. H. Fredrickson, *Phys. Today*, 1999, **52**, 32–38.

32 S. Lee, M. J. Bluemle and F. S. Bates, *Science*, 2010, **330**, 349–353.

33 S. H. Choi, F. S. Bates and T. P. Lodge, *Macromolecules*, 2014, **47**, 7978–7986.

34 T. M. Gillard, S. Lee and F. S. Bates, *Proc. Natl Acad. Sci. USA*, 2016, **113**, 5167–5172.

35 S. Chanpuriya, K. Kim, J. Zhang, S. Lee, A. Arora, K. D. Dorfman, K. T. Delaney, G. H. Fredrickson and F. S. Bates, *ACS Nano*, 2016, **10**, 4961–4972.

36 M. Liu, Y. Qiang, W. Li, F. Qiu and A. C. Shi, *ACS Macro Lett.*, 2016, **5**, 1167–1171.

37 W. Li, C. Duan and A. C. Shi, *ACS Macro Lett.*, 2017, **6**, 1257–1262.

38 K. Kim, M. W. Schulze, A. Arora, R. M. Lewis III, M. A. Hillmyer, K. D. Dorfman and F. S. Bates, *Science*, 2017, **356**, 520–523.

39 K. Kim, A. Arora, R. M. Lewis, M. Liu, W. Li, A.-C. Shi, K. D. Dorfman and F. S. Bates, *Proc.*

Natl. Acad. Sci. USA, 2018, **115**, 847–854.

40 D. V. Perroni and M. K. Mahanthappa, *Soft Matter*, 2013, **9**, 7919–7922.

41 K. Yue, M. Huang, R. L. Marson, J. He, J. Huang, Z. Zhou, J. Wang, C. Liu, X. Yan, K. Wu, Z. Guo, H. Liu, W. Zhang, P. Ni, C. Wesdemiotis, W.-B. Zhang, S. C. Glotzer and S. Z. D. Cheng, *Proc. Natl. Acad. Sci. USA*, 2016, **113**, 14195–14200.

42 S. A. Kim, K.-J. Jeong, A. Yethiraj and M. K. Mahanthappa, *Proc. Natl. Acad. Sci. USA*, 2017, **114**, 4072–4077.

43 F. C. Frank and J. S. Kasper, *Acta Crystallogr.*, 1958, **11**, 184–190.

44 F. C. Frank and J. S. Kasper, *Acta Crystallogr.*, 1959, **12**, 483–499.

45 M. Peterca and V. Percec, *Science*, 2010, **330**, 333–334.

46 A. F. Schuch and R. L. Mills, *J. Chem. Phys.*, 1970, **52**, 6000.

47 D. T. Cromer, R. L. Mills, D. Schiferl and L. A. Schwalbe, *Acta Crystallogr. Sect. B Struct. Crystallogr. Cryst. Chem.*, 1981, **37**, 8–11.

48 S. Nosé and M. L. Klein, *Phys. Rev. Lett.*, 1983, **50**, 1207–1210.

49 S. Buchsbaum, R. L. Mills and D. Schiferl, *J. Phys. Chem.*, 1984, **88**, 2522–2525.

50 R. L. Mills, B. Olinger and D. T. Cromer, *J. Chem. Phys.*, 1986, **84**, 2837.

51 D. Tomasino, Z. Jenei, W. Evans and C.-S. Yoo, *J. Chem. Phys.*, 2014, **140**, 244510.

52 M. L. Klein, D. Levesque and J.-J. Weis, *Phys. Rev. B*, 1980, **21**, 5785–5792.

53 B. J. Baer and M. Nicol, *J. Phys. Chem.*, 1990, **94**, 1073–1078.

54 D. Sihachakr and P. Loubeyre, *Phys. Rev. B*, 2004, **70**, 134105.

55 Y. Akahama, T. Maekawa, T. Sugimoto, H. Fujihisa, N. Hirao and Y. Ohishi, *J. Phys. Conf. Ser.*, 2014, **500**, 182001.

56 B. M. Rosen, C. J. Wilson, D. A. Wilson, M. Peterca, M. R. Imam and V. Percec, *Chem. Rev.*, 2009, **109**, 6275–6540.

57 H.-J. Sun, S. Zhang and V. Percec, *Chem. Soc. Rev.*, 2015, **44**, 3900–3923.

58 Committee on Synthetic Hierarchical Structures, in *Hierarchical structures in biology as a guide for new materials technology*, ed. D. A. Tirrell, National Academy Press, Washington, DC, 1994, pp. 17–38.

59 G. M. Whitesides and B. Grzybowski, *Science*, 2002, **295**, 2418–2421.

60 S. B. Prusiner, *Science*, 1982, **216**, 136–144.

61 S. B. Prusiner, *Science*, 1991, **252**, 1515–1522.

62 K. M. Pan, M. Baldwin, J. Nguyen, M. Gasset, A. Serban, D. Groth, I. Mehlhorn, Z. Huang, R. J. Fletterick, F. E. Cohen and S. B. Prusiner, *Proc. Natl. Acad. Sci. USA*, 1993, **90**, 10962–10966.

63 S. B. Prusiner, *Proc. Natl. Acad. Sci. USA*, 1998, **95**, 13363–13383.

64 J. King, C. Haase-Pettingell and D. Gossard, *Am. Sci.*, 2002, **90**, 445–453.

65 E. T. Powers and D. L. Powers, *Biophys. J.*, 2008, **94**, 379–391.

66 C. J. Kawa, *J. Chem. Educ.*, 1988, **65**, 884–885.

67 D. J. P. Yeardley, G. Ungar, V. Percec, M. N. Holerca and G. Johansson, *J. Am. Chem. Soc.*, 2000, **122**, 1684–1689.

68 H. Duan, S. D. Hudson, G. Ungar, M. N. Holerca and V. Percec, *Chem. Eur. J.*, 2001, **7**, 4134–4141.

69 D. R. Dukeson, G. Ungar, V. S. K. Balagurusamy, V. Percec, G. A. Johansson and M. Glodde, *J. Am. Chem. Soc.*, 2003, **125**, 15974–15980.

70 V. S. K. Balagurusamy, G. Ungar, V. Percec and G. Johansson, *J. Am. Chem. Soc.*, 1997, **119**, 1539–1555.

71 P. Sakya, J. M. Seddon, R. H. Templer, R. J. Mirkin and G. J. T. Tiddy, *Langmuir*, 1997, **13**, 3706–3714.

72 B. M. Rosen, D. A. Wilson, C. J. Wilson, M. Peterca, B. C. Won, C. Huang, L. R. Lipski, X. Zeng, G. Ungar, P. A. Heiney and V. Percec, *J. Am. Chem. Soc.*, 2009, **131**, 17500–17521.

73 M. Peterca, M. R. Imam, C.-H. Ahn, V. S. K. Balagurusamy, D. A. Wilson, B. M. Rosen and V. Percec, *J. Am. Chem. Soc.*, 2011, **133**, 2311–2328.

74 D. L. D. Caspar, *Biophys. J.*, 1980, **32**, 103–135.

75 V. Percec, C.-H. Ahn, G. Ungar, D. J. P. Yeardley, M. Möller and S. S. Sheiko, *Nature*, 1998, **391**, 161–164.

76 V. Percec, M. R. Imam, M. Peterca, D. A. Wilson and P. A. Heiney, *J. Am. Chem. Soc.*, 2009, **131**, 1294–1304.

77 V. Percec, M. R. Imam, M. Peterca, D. A. Wilson, R. Graf, H. W. Spiess, V. S. K. Balagurusamy and P. A. Heiney, *J. Am. Chem. Soc.*, 2009, **131**, 7662–7677.

78 G. Ungar, V. Percec, M. Holerca, G. Johansson and J. Heck, *Chem. Eur. J.*, 2000, **6**, 1258–1266.

79 V. Percec, W. Cho, M. Möller, S. A. Prokhorova, G. Ungar and D. J. P. Yeardley, *J. Am. Chem. Soc.*, 2000, **122**, 4249–4250.

80 M. Peterca, V. Percec, M. R. Imam, P. Leowanawat, K. Morimitsu and P. A. Heiney, *J. Am. Chem. Soc.*, 2008, **130**, 14840–14852.

Table of Contents Abstract Graphic and Text

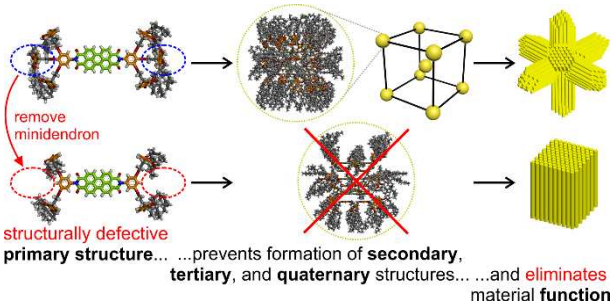

Comparing the self-organization of two dendronized perylene bisimides reveals how structurally defective primary structure eliminates memory function *via* hierarchical self-organization.